Nonlinear Dyn (2020) 99:2785–2799
https://doi.org/10.1007/s11071-020-05481-1

ORIGINAL PAPER

Super-twisting sliding mode control for aircraft at high angle of attack based on finite-time extended state observer

Junjie Liu · Mingwei Sun · Zengqiang Chen · Qinglin Sun

Received: 12 May 2019 / Accepted: 10 January 2020 / Published online: 28 January 2020

Abstract This paper proposes a finite-time decoupling control strategy for aircraft with thrust vector at high angle of attack maneuver. Firstly, the nonlinear mathematical model of the aircraft is presented. Taking into account the insufficiency of the aerodynamic control surface, a thrust vector model with double nozzles is added. Subsequently, a three-channel decoupling control scheme based on finite-time extended state observer is employed to realize the high angle of attack maneuver. Strong coupling among different channels, aerodynamic uncertainties and other unmodeled dynamics are regarded as total disturbance and estimated by a finite-time extended state observer. Super-twisting (SWT) sliding mode control is utilized to obtain expected performance and finite-time stability. The daisy chain method is adopted to realize the control allocation. Finally, the numerical simulations are provided to demonstrate the effectiveness and robustness of the proposed methodology.

Keywords Aircraft nonlinear dynamic model · High angle of attack · Finite-time extended state observer · Super-twisting slide mode control · Thrust vector · Robustness

J. Liu · M. Sun · Z. Chen (✉) · Q. Sun
College of Artificial Intelligence, Nankai University, Tianjin 300350, China
e-mail: chenzq@nankai.edu.cn

1 Introduction

With the envelope extension and enhanced agility of fighter aircraft, higher flight performances are in urgent demand [1]. The super maneuverability has become one of the major features of modern advanced fighter aircraft, which can improve attack ability and survival chance. The super maneuverability means that the fighter aircraft can complete fast maneuver action with high angular rate at high angle of attack (AOA). The thrust vector technology usually needs to be adopted due to the low efficiency of aerodynamic control surfaces at high AOA [2,3]. Moreover, the deep stall caused by high AOA makes the fighter aircraft unstable and difficult to control. Especially, in super maneuvering, the air flowing through the aircraft changes from the attached flow to the vortex flow. Then, the vortex breakdowns in a row and finally becomes the separated flow. This process generates unsteady aerodynamic force leading to strong nonlinearity, coupling, uncertainty and hysteresis in the fighter aircraft [4]. All these problems lead to a great challenge for controllers design for fighter aircraft.

For flight controller design, the linear control methods such as gain scheduling, pole placement, optimal control and H_∞ control [5–7] are traditionally used. However, it is relatively difficult for these methods to cover a large flight envelope. Furthermore, the linear models and linear control methods will no longer be suitable when the aircrafts fly at high angle of attack

or roll with a high rate. Thus, the nonlinear control strategy needs to be developed. In order to solve these problems and overcome the limitations of linear controllers, the nonlinear dynamic inversion (NDI) is performed [8–10]. The NDI method can decouple the system dynamics by canceling the nonlinear functions of the nonlinear model, but the premise is that the dynamics must be known accurately. Some nonlinear adaptive flight controllers based on back-stepping control method are designed to eliminate parameter uncertainties and nonlinear factor [11–13]. However, these adaptive flight controllers are not simple because a large number of aerodynamic parameters usually need to be estimated, which is difficult to apply to practical flight at high AOA. In addition, these control strategies are all based on the idea of multivariable design, which is difficult to perform stability analysis as single-input-single-output (SISO) system. Active disturbance rejection control (ADRC) is a novel control method proposed by Han [14], which is not model based. As the core part of ADRC, the extended state observer (ESO) can regard the channels coupling, unmodeled dynamics and external disturbance as generalized disturbance and estimate it, which then can be compensated in real time [15–19]. Such control idea can provide a new three-channel controller design independently in the presence of aerodynamic uncertainties, strong couplings and nonlinearity. At high angle of attack, the robustness of the control system for aircraft is vitally important. The ESO with finite-time convergence is more suitable for flight control design than the conventional ESO. Thus, it is of practical significance to expand the conventional ESO to finite-time ESO and apply it to flight system design.

Compared to asymptotically stabilizing control systems, the finite-time stabilizing controllers usually show stronger robustness properties [20]. Especially, the flight controller with finite-time convergence can produce stronger robustness in the presence of strong couplings and aerodynamic uncertainties. Sliding mode control (SMC) is a robust technique to control nonlinear systems in the presence of uncertainty conditions [21], and higher-order SMC has been proposed to reduce its chattering phenomenon [22,23]. The super-twisting algorithm (STA) is a well-known second-order sliding mode algorithm introduced in [24], and its finite-time convergence and robustness have been analyzed [25–27]. Due to its excellent finite-time convergence, the STA is widely utilized to design controllers [28–32], differentiators [33,34] and observers [28,35]. Furthermore, the finite-time control laws for flight control system in the presence of uncertainties were developed [20,36–40]. Especially, reference [38] designed the super-twisting controllers to realize the roll-coupling maneuver by aerodynamic surfaces. However, the authors do not take the maneuver at high angle of attack with thrust vector into account. At high angle of attack, the effectiveness of the aerodynamic control surfaces degrades significantly so that the thrust vector usually needs to be employed. Thus, the finite-time controllers based on super-twisting algorithm and finite-time ESO can be considered to realize the super maneuvers at high angle of attack for the aircraft with thrust vector.

Motivated by the extended state observer principle and the finite-time control methodologies, this paper presents a high angle of attack finite-time control strategy based on finite-time extended state observer (FTESO) and super-twisting sliding mode control method for fighter aircraft. The main contributions of this paper can be summarized as follows:

(1) Compared with the conventional extended state observer with asymptotic convergence, the FTESO has an upper bound of convergence time and produces stronger robustness. Thus, the FTESO can be used to estimate the state and total disturbance more effectively, which will improve the observing and disturbance rejection ability of the flight control system for aircraft at high AOA.
(2) For high AOA control of fighter aircraft, the traditional multivariable decoupling control is often used, which leads to a controversial issue that it is difficult to carry out stability margin analysis like a SISO system. By employing FTESO, the independent controllers for three channels are designed, respectively to eliminate the strong couplings of interchannels. Instead of the traditional multivariable decoupling control, such control strategy is more conducive to controller implementation in practical flight.
(3) The original system dynamic is reduced to a unit integrator system based upon FTESO. The super-twisting sliding mode control method can then be employed to achieve the finite convergence of feedback error and the expected control performance.

The remaining parts of this paper are organized as follows: Sect. 2 describes the aircraft dynamic model with

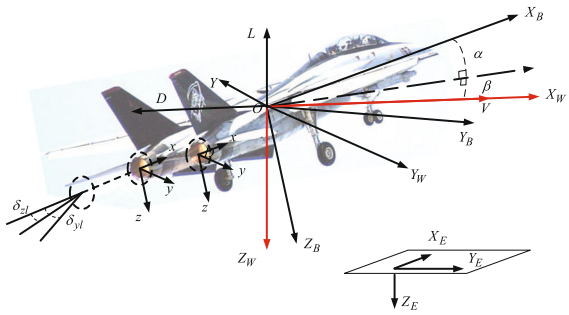

Fig. 1 Aircraft model and thrust vector diagram

thrust vector; Sect. 3 presents the proposed control strategy and control allocation process; Sect. 4 gives the simulation results and robustness verification; and the conclusions are provided in Sect. 5.

2 The problem statement and the aircraft model

The mathematical model of the aircraft comes from a benchmark mathematical model [12]. In order to avoid the singularity due to the high angle of attack, a mathematical model based on the track coordinate system is derived. In addition, the thrust vector technology needs to be adopted owing to the poor control effectiveness of aerodynamic actuators. Therefore, a mathematical model with thrust vector model is presented first. The aircraft and coordinate diagram is shown in Fig. 1. The meaning of nomenclature and variables can be found in "Appendix."

2.1 Nonlinear dynamic model

$$\dot{V} = \frac{1}{m}[-D + Y\sin(\beta) - mg\sin(\gamma)] + \frac{1}{m}[T_x\cos(\beta)\cos(\alpha) + T_y\sin(\beta) + T_z\cos(\alpha)\sin(\beta)] \tag{1}$$

$$\dot{\alpha} = q - \tan(\beta)[p\cos(\alpha) + r\sin(\alpha)] + \frac{1}{mV\cos(\beta)}[-L + mg\cos(\gamma)\cos(\mu)] + \frac{1}{mV\cos(\beta)}[-T_x\sin(\alpha) + T_z\cos(\alpha)] \tag{2}$$

$$\dot{\beta} = -r\cos(\alpha) + p\sin(\alpha) + \frac{1}{mV}[Y\cos(\beta) + mg\cos(\gamma)\sin(\mu)] + \frac{1}{mV}[-T_x\sin(\beta)\cos(\alpha) + T_y\cos(\beta) - T_z\sin(\beta)\sin(\alpha)] \tag{3}$$

$$\dot{\gamma} = \frac{1}{mV}[L\cos(\mu) - Y\sin(\mu)\cos(\beta)] - \frac{T_y}{mV}\cos(\beta) + \frac{T_x}{mV}[\sin(\mu)\sin(\beta)\cos(\alpha) + \cos(\mu)\sin(\alpha)] + \frac{T_z}{\sin(\alpha)}[\sin(\mu)\sin(\beta)\sin(\alpha) - \cos(\mu)\cos(\alpha)] \tag{4}$$

$$\dot{\chi} = \frac{1}{mv\cos(\gamma)}[L\sin(\mu) + Y\cos(\mu)\cos(\beta)] + \frac{T_y}{mv\cos(\gamma)}\cos(\mu)\cos(\beta) + \frac{T_x}{mV\cos(\gamma)}[\sin(\mu)\sin(\alpha) - \cos(\mu)\sin(\beta)\cos(\alpha)] - \frac{T_z}{mV\cos(\gamma)}[\cos(\mu)\sin(\beta)\sin(\alpha) + \sin(\mu)\cos(\alpha)] \tag{5}$$

$$\dot{\mu} = \frac{1}{\cos(\beta)}[p\cos(\alpha) + r\sin(\alpha)] + \frac{L}{mV}[\tan(\gamma)\sin(\mu) + \tan(\beta)] + \frac{Y + T_y}{mV}\tan(\gamma)\cos(\mu)\cos(\beta) - \frac{g}{V}(\cos(\gamma)\cos(\mu)\tan(\beta)) + \frac{T_x\sin(\alpha) - T_z\cos(\alpha)}{mV}[\tan(\gamma)\sin(\mu) + \tan(\beta)] - \frac{T_x\cos(\alpha) + T_z\sin(\alpha)}{mV}[\tan(\gamma)\cos(\mu)\sin(\beta)] \tag{6}$$

$$\dot{p} = \frac{I_{zz}(l_a + l_T) + I_{xz}(n_a + n_T)}{I_{xx}I_{zz} - I_{xz}^2} + \frac{I_{xz}(I_{xx} - I_{yy} + I_{zz})}{I_{xx}I_{zz} - I_{xz}^2}pq + \frac{I_{zz}(I_{yy} - I_{zz}) - I_{xz}^2}{I_{xx}I_{zz} - I_{xz}^2}qr \tag{7}$$

$$\dot{q} = \frac{(m_a + m_T) + (I_{zz} - I_{xx})pr + I_{xz}(r^2 - p^2)}{I_{yy}} \tag{8}$$

$$\dot{r} = \frac{I_{xz}(l_a + l_T) + I_{xx}(n_a + n_T)}{I_{xx}I_{zz} - I_{xz}^2} + \frac{I_{xx}(I_{xx} - I_{yy}) + I_{zz}^2}{I_{xx}I_{zz} - I_{xz}^2}pq - \frac{I_{xz}(I_{xx} - I_{yy} + I_{zz})}{I_{xx}I_{zz} - I_{xz}^2}qr \tag{9}$$

$$\dot{x}_E = V\cos(\gamma)\cos(\chi) \tag{10}$$

$$\dot{y}_E = V\cos(\gamma)\sin(\chi) \tag{11}$$

$$\dot{z}_E = -V\sin(\gamma) \tag{12}$$

D, Y, L represent aerodynamic drag, lateral force and lift force, respectively, and can be obtained by

$$\begin{bmatrix} D \\ Y \\ L \end{bmatrix} = \begin{bmatrix} -\cos\alpha\cos\beta & -\sin\beta & -\sin\alpha\cos\beta \\ -\cos\alpha\sin\beta & \cos\beta & -\sin\alpha\sin\beta \\ \sin\alpha & 0 & -\cos\alpha \end{bmatrix} \begin{bmatrix} \bar{q}SC_{x\_\text{tot}} \\ \bar{q}SC_{y\_\text{tot}} \\ \bar{q}SC_{z\_\text{tot}} \end{bmatrix} \tag{13}$$

and the aerodynamic torque can be obtained by

$$\begin{bmatrix} l_a \\ m_a \\ n_a \end{bmatrix} = \begin{bmatrix} \bar{q}SbC_{l\_\text{tot}} \\ \bar{q}ScC_{m\_\text{tot}} \\ \bar{q}SbC_{n\_\text{tot}} \end{bmatrix} \tag{14}$$

$C_{i\_\text{tot}}(i = x, y, z)$ and $C_{j\_\text{tot}}(j = l, m, n)$ denote the total aerodynamic force and torque coefficients, respectively, which are nonlinear functions for α, β and the aerodynamic control surfaces $\delta_i(i = e, a, r)$, and can be obtained by interpolation and calculation. Taking C_{x_tot} as an example, its computational formula can be expressed as

$$\begin{aligned} C_{x\_\text{tot}} =& C_x(\alpha, \beta, \delta_e) + \Delta C_{x,\text{lef}}\left(1 - \frac{\delta_{\text{lef}}}{25}\right) + \Delta C_{x,sb}(\alpha) \\ & \left(\frac{\delta_s b}{60}\right) + \frac{\bar{c}q}{2V}\left[C_{x,q}(\alpha) + \Delta C_{x,\text{lef}}(\alpha)\left(1 - \frac{\delta_{\text{lef}}}{25}\right)\right] \end{aligned} \tag{15}$$

where C_x represents the x-axis force coefficient along positive x body axis, δ_{lef} is the leading-edge flap deflection and $C_{x,q} = \frac{\partial C_x}{\partial(\bar{c}q/(2V))}$. $\Delta C_{x,\text{lef}}$ can be calculated by $\Delta C_{x,\text{lef}} = C_{x,\text{lef}}(\alpha, \beta) - C_x(\alpha, \beta, \delta_e = 0)$. Considering the page limitation, the rest of the expression of total aerodynamic force or torque coefficients can be found in [41].

2.2 The thrust vector model

Two engines with rotatable nozzles are installed in the rear symmetrically, which can deflect [−20°,20°] in the yaw and pitch directions, respectively. The angle between the projection of the vector nozzle axis in the plane of symmetry of the aircraft and the longitudinal axis of the body is defined as the pitch deflection angle, which can be represented by δ_{zi} ($i = l, r$ denotes the rotatable nozzles on the left and right, respectively). Similarly, the angle between the vector nozzle axis and the plane of symmetry of the aircraft can be defined as the yaw deflection angle δ_{yi}. The two nozzles can generate the desired three-axis torques by different deflection combinations, and the corresponding total deflection angles in the roll, yaw and pitch channels can be produced as

$$\begin{cases} \delta_x = \frac{-\delta_{zl} + \delta_{zr}}{2} \\ \delta_y = \frac{\delta_{yl} + \delta_{yr}}{2} \\ \delta_z = \frac{\delta_{zl} + \delta_{zr}}{2} \end{cases}. \tag{16}$$

The thrust components of any engine along the three-axis in the body coordinate system can be expressed as

$$\boldsymbol{T}_{fi} = \begin{bmatrix} T_{xi} \\ T_{yi} \\ T_{zi} \end{bmatrix} = \zeta_{fi} T_i \begin{bmatrix} \cos(\delta_{yi})\cos(\delta_{zi}) \\ \sin(\delta_{yi}) \\ -\cos(\delta_{yi})\sin(\delta_{zi}) \end{bmatrix}. \tag{17}$$

where ζ_{fi} is the thrust coefficient. Assume that $\zeta_{fr} = \zeta_{fl}$, $T_r = T_l$, $\delta_{yr} = \delta_{yl} = \delta_y$. Then, the thrust components can be expressed as

$$\begin{aligned} \begin{bmatrix} T_x \\ T_y \\ T_z \end{bmatrix} &= \boldsymbol{T}_{fl} + \boldsymbol{T}_{fr} \\ &= \zeta_f T \begin{bmatrix} \cos(\delta_x)\cos(\delta_y)\cos(\delta_z) \\ \sin(\delta_y) \\ -\cos(\delta_x)\cos(\delta_y)\sin(\delta_z) \end{bmatrix} \end{aligned} \tag{18}$$

where $T_j(j = x, y, z)$ is the engine thrust component along the three axes in the body-fixed axis, T is the total engine thrust, and the ζ_f is thrust coefficient, which indicates the engine thrust loss. In order to simplify the model, when the thrust vector deflection angle is small (less than 20°), Eq. (13) can be represented approximately as

$$\begin{bmatrix} T_x \\ T_y \\ T_z \end{bmatrix} = \zeta_f T \begin{bmatrix} 1 \\ \delta_y \\ -\delta_z \end{bmatrix}. \tag{19}$$

Define x_T, y_T, z_T as the engine position in the body-fixed axis and the torque expression can be described as

$$\begin{bmatrix} l_T \\ m_T \\ n_T \end{bmatrix} = \begin{bmatrix} x_T \\ y_T \\ z_T \end{bmatrix} \otimes \begin{bmatrix} T_x \\ T_y \\ T_z \end{bmatrix}. \tag{20}$$

3 Control strategy

In this section, the super-twisting sliding mode control scheme based on FTESO for the nonlinear dynamic model with thrust vector is presented. The angular variables α, β and the angular rates p, q, r are selected as control variables. Independent SISO controllers for α, β and p are designed, respectively. The entire control

structure is illustrated in Fig. 2. α_d, β_d, p_d are the reference commands, and T_c represents the thrust command. δ_e, δ_a, δ_r represent the deflection angle of the elevator, aileron and rudder, respectively. δ_x, δ_y, δ_z represent the corresponding deflection angle of the vector nozzles. In high AOA maneuver, the maximum thrust is used. The specific design process is as follows.

3.1 The finite-time extended state observer

Considering the following system

$$\dot{x} = f(x(t)),\ f(0) = 0, x \in \mathcal{R}^n, x(0) = x_0, \tag{21}$$

where $f : \mathcal{R}^n \longrightarrow \mathcal{R}^n$ is a nonlinear function.

Definition 1 [42]. The origin of system Eq. (21) is a finite-time stable equilibrium if the origin is Lyapunov stable, then there exits a settling time function $T_{fi} : \mathcal{R}^n \longrightarrow \mathcal{R}^n$, such that for every $x_0 \in \mathcal{R}^n$, the solution $x(t, x_0)$ of Eq. (21) satisfies $\lim_{t \to T_{fi}(x_0)} x(t, x_0) = 0$.

Lemma 1 [43]. *Suppose there exits a continuous function $V : D \longrightarrow \mathcal{R}$ such that the following conditions hold: (1) V is positive definite; (2) there exist real number $c > 0$ and $\theta \in (0, 1)$ and an open neighborhood $U \subset D$ of the origin such that*

$$\dot{V}(x) + c(V(t))^{\theta} \leq 0, x \in U \backslash \{0\} \tag{22}$$

Then, the origin is a finite-time stable equilibrium of system Eq. (21), and the settling time function T_{fi} is

$$T_{fi} \leq \frac{1}{c(1-\theta)} (V(x))^{(1-\theta)} \tag{23}$$

where T_{fi} is continuous. If in addition $D = \mathcal{R}^n$, V is proper, and $\dot{V}$ takes negative values on $\mathcal{R}^n \backslash \{0\}$, then the origin is a globally finite-time stable equilibrium of system Eq. (21).

Consider a second-order plant, described by a second-order nonlinear differential equation with unknown dynamics and external disturbance

$$\ddot{y}(t) = f\ (y(t), \dot{y}(t), w(t)) + bu(t), \tag{24}$$

where $u(t)$, $y(t)$ and $w(t)$ are the input, the output and the external disturbance of the system, respectively. b denotes the given input gain. For the given second-order system, we can rewrite Eq. (24) as

$$\begin{aligned} \ddot{y}(t) &= f\ (y(t), \dot{y}(t), w(t)) + (b - b_0)u(t) + b_0 u \\ &= f + b_0 u \end{aligned} \tag{25}$$

where $f = f\ (y(t), \dot{y}(t), w(t)) + (b - b_0)u(t)$ is referred to as the generalized disturbance or total disturbance including the unknown internal dynamics and the external disturbance. b_0 is an adjustable parameter related to b. The basic idea is to obtain an estimation of f , that is $\hat{f}$. And then, if the control law $u = (u_0 - \hat{f})/b_0$ is used, the original system (24) will be expressed by a unit-gain integrator system plus a disturbance $(f - \hat{f})$. That is

$$\ddot{y}(t) = u_0 + (f - \hat{f}) \tag{26}$$

The disturbance $(f - \hat{f})$ makes the real plant deviate from the anticipated integrator system. When f can be estimated exactly, the original system (24) will be reduced to

$$\ddot{y}(t) = u_0 \tag{27}$$

For the system as (27), the expected performance can be easily obtained by designing proper control law u_0. In order to obtain $\hat{f}$, we can rewrite (25) in state equation form

$$\begin{cases} \dot{x}_1 = x_2 \\ \dot{x}_2 = x_3 + b_0 u \\ \dot{x}_3 = H \\ y = x_1 \end{cases} \tag{28}$$

where $x_3 = f, H = \dot{f}$. Define $\hat{x}_i (i = 1, 2, 3)$ as an estimation of $x_i (i = 1, 2, 3)$, the estimation error $e = [e_1, e_2, e_3]^{\mathrm{T}} = [\hat{x}_1, \hat{x}_2, \hat{x}_3]^{\mathrm{T}} - [x_1, x_2, x_3]^{\mathrm{T}}$, then the state observer can be constructed as

$$\begin{cases} \dot{\hat{x}}_1 = \hat{x}_2 - \beta_{01}\varphi(\hat{x}_1 - x_1) \\ \dot{\hat{x}}_2 = \hat{x}_3 - \beta_{02}\varphi(\hat{x}_1 - x_1) + b_0 u \\ \dot{\hat{x}}_3 = -\beta_{03}\varphi(\hat{x}_1 - x_1) \end{cases} \tag{29}$$

where $\varphi(\cdot)$ is a function about the estimation error, $l_i > 0 (i = 1, 2, 3)$ represents the adjustable observer gain. $\hat{x}_1$ and $\hat{x}_2$ can provide the estimation of x_1 and x_2. More importantly, $\hat{x}_3$ can estimate the total disturbance f. Then, the estimation error dynamic can be expressed as

$$\begin{cases} \dot{e}_1 = e_2 - \beta_1\varphi(e_1) \\ \dot{e}_2 = e_3 - \beta_2\varphi(e_1) \\ \dot{e}_3 = -\beta_3\varphi(e_1) - h \end{cases} \tag{30}$$

When $\varphi(e)$ are chosen as linear form, that is $\varphi(e) = e$, the extended state observer can be described as

$$\begin{cases} \dot{\hat{x}}_1 = \hat{x}_2 - \beta_{01}(\hat{x}_1 - x_1) \\ \dot{\hat{x}}_2 = \hat{x}_3 - \beta_{02}(\hat{x}_1 - x_1) + b_0 u, \\ \dot{\hat{x}}_3 = -\beta_{03}(\hat{x}_1 - x_1) \end{cases} \tag{31}$$

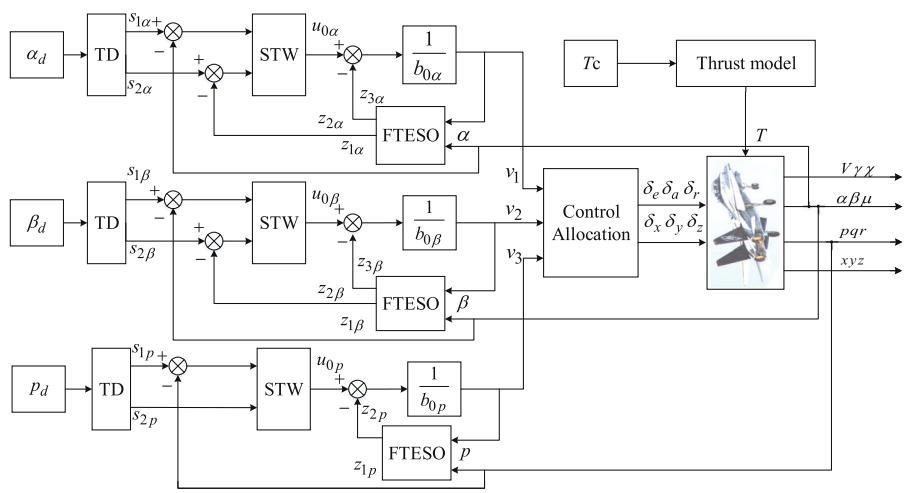

Fig. 2 Super-twisting control structure based on FTESO

which is called linear extended state observer (LESO). Motivated by the finite-time stable system

$$\dot{e} = -k\mathrm{sgn}(e)\,|e|^{\kappa}\,, \kappa \in (0,\,1)$$

and the continuous smooth tracking differentiator in reference [34], a finite-time convergent extended state observer can be constructed as

$$\begin{cases} \dot{e}_1 = e_2 - \beta_{01}|e_1|^{\frac{\kappa+1}{2}}\mathrm{sgn}(e_1) \\ \dot{e}_2 = e_3 - \beta_{02}|e_1|^{\frac{\kappa+1}{2}}\mathrm{sgn}(e_1) \\ \dot{e}_3 = -\beta_{03}|e_1|^{\kappa}\mathrm{sgn}(e_1) - H \end{cases} \tag{32}$$

Assumption 1 For the dynamic system as Eq. (32), the total disturbance f is continuously differentiable and its differential H is bounded, which satisfies $|H| < H_M$.

Theorem 1 *For the dynamic system* (24)*, if the extended state observer as Eq.* (31) *is designed, then there exit constant number* $0 < \kappa < 1$*,* $\beta_{0i}(i = 1, 2, 3) > 0$ *and* $\beta_{01}\beta_{02}\frac{\kappa+1}{2} - \beta_{03} > 0$*, the state variables* x_1 *and* x_2 *can be estimated within a finite time* T_{fi}*. Moreover, the estimation error of total disturbance can also converge to a neighborhood of the origin in finite time.*

Proof For the error dynamic system in Eq. (32), define

$$\varsigma = [|e_1|^{\frac{\kappa+1}{2}}\mathrm{sgn}(e_1) \quad e_2 \quad e_3]^{\mathrm{T}}$$

$$P = \begin{bmatrix} \frac{2\beta_{01}}{\alpha+1} + \beta_{02}^2 + \beta_{03}^2 & -\beta_{02} & -\beta_{03} \\ -\beta_{02} & 2 & 0 \\ -\beta_{03} & 0 & 2 \end{bmatrix}$$

Then, a Lyapunov candidate function can be chosen as

$$V(\beta_{0i}, \varsigma) = \varsigma^{\mathrm{T}} P \varsigma \tag{33}$$

When $\beta_{0i} > 0$, P is a symmetric positive definite matrix. Let λ represent eigenvalue sequence, we can obtain

$$\lambda_{\min}\{P\}\,\|\varsigma\|_2^2 \le V \le \lambda_{\max}\{P\}\,\|\varsigma\|_2^2 \tag{34}$$

where $\|\varsigma\|_2^2 = |e_1|^{\kappa+1} + e_2^2 + e_3^2$, and

$$|e_1|^{\frac{\kappa+1}{2}} \le \|\varsigma\|_2 \le \sqrt{\frac{V}{\lambda_{\min}\{P\}}} \tag{35}$$

Derivative V, that is

$$\begin{aligned} \dot{V} =& [|e_1|^{\frac{\kappa+1}{2}}\mathrm{sgn}(e_1) \quad e_2 \quad e_3]Q \\ & \cdot [|e_1|^{\frac{\kappa+1}{2}}\mathrm{sgn}(e_1) \quad e_2 \quad e_3]^{\mathrm{T}} \\ & + 2H(\beta_{03}|e_1|^{\frac{\kappa+1}{2}}\mathrm{sgn}(e_1) + 2e_3) \\ =& -\varsigma^{\mathrm{T}} Q \varsigma + 2H(\beta_{03}|e_1|^{\frac{\kappa+1}{2}}\mathrm{sgn}(e_1) + 2e_3) \\ =& V_1 + V_2 \end{aligned} \tag{36}$$

$$Q = \begin{bmatrix} -\beta_{01}(\kappa+1)(\frac{2\beta_{01}}{\kappa+1} + \beta_{02}^2 + \beta_{03}^2)|e_1|^{\frac{\kappa-1}{2}} + 2\beta_{03}^2|e_1|^{\frac{\kappa-1}{2}} + 2\beta_{02}^2\ \frac{\kappa+1}{2}|e_1|^{\frac{\kappa-1}{2}}(\frac{2\beta_{01}}{\kappa+1} + \beta_{02}^2 + \beta_{03}^2 + \beta_{01}\beta_{02}) - 2\beta_{02}\ \beta_{01}\beta_{03}\frac{\kappa+1}{2}|e_1|^{\frac{\kappa-1}{2}} - 2\beta_{03}|e_1|^{\frac{\kappa-1}{2}} - \beta_{02} \\ \frac{\kappa+1}{2}|e_1|^{\frac{\kappa-1}{2}}(\frac{2\beta_{01}}{\kappa+1} + \beta_{02}^2 + \beta_{03}^2 + \beta_{01}\beta_{02}) - 2\beta_{02} \quad -\beta_{02}(\kappa+1)|e_1|^{\frac{\kappa-1}{2}} \quad -\beta_{03}\frac{\kappa+1}{2}|e_1|^{\frac{\kappa-1}{2}} + 2 \\ \beta_{01}\beta_{03}\frac{\kappa+1}{2}|e_1|^{\frac{\kappa-1}{2}} - 2\beta_{03}|e_1|^{\frac{\kappa-1}{2}} - \beta_{02} \quad -\beta_{03}\frac{\kappa+1}{2}|e_1|^{\frac{\kappa-1}{2}} + 2 \quad 0 \end{bmatrix}. \ \square$$

where Q is symmetric and can be equivalent to

$$A^T P + PA = -Q \tag{37}$$

where

$$\begin{aligned} A &= \begin{bmatrix} -\beta_{01}\frac{\kappa+1}{2}|e_1|^{\frac{\kappa-1}{2}} & \frac{\kappa+1}{2}|e_1|^{\frac{\kappa-1}{2}} & 0 \\ -\beta_{02} & 0 & 1 \\ -\beta_{03}|e_1|^{\frac{\kappa-1}{2}} & 0 & 0 \end{bmatrix} \\ &= \begin{bmatrix} -\frac{\kappa+1}{2}|e_1|^{\frac{\kappa-1}{2}} & 0 & 0 \\ 0 & -1 & 0 \\ 0 & 0 & -|e_1|^{\frac{\kappa-1}{2}} \end{bmatrix} \begin{bmatrix} \beta_{01} & -1 & 0 \\ \beta_{02} & 0 & -1 \\ \beta_{03} & 0 & 0 \end{bmatrix}. \end{aligned} \tag{38}$$

According to Eq. (38), we can obtain

$$\begin{aligned} |sI - A| &= \begin{vmatrix} s + \beta_{01}\frac{\kappa+1}{2}|e_1|^{\frac{\kappa-1}{2}} & -\frac{\kappa+1}{2}|e_1|^{\frac{\kappa-1}{2}} & 0 \\ \beta_{02} & s & -1 \\ \beta_{03}|e_1|^{\frac{\kappa-1}{2}} & 0 & s \end{vmatrix} \\ &= s^2\left(s + \beta_{01}\frac{\kappa+1}{2}|e_1|^{\frac{\kappa-1}{2}}\right) \\ &\quad + \frac{\kappa+1}{2}|e_1|^{\frac{\kappa-1}{2}}\left(\beta_{02}s + \beta_{03}|e_1|^{\frac{\kappa-1}{2}}\right) \\ &= s^3 + \beta_{01}\frac{\kappa+1}{2}|e_1|^{\frac{\kappa-1}{2}}s^2 \\ &\quad + \beta_{02}\frac{\kappa+1}{2}|e_1|^{\frac{\kappa-1}{2}}s + \beta_{03}\frac{\kappa+1}{2}|e_1|^{\kappa-1} \end{aligned} \tag{39}$$

From Eq. (39), the polynomial coefficients are all positive. If β_{01}, β_{02}, β_{03}, κ are chosen properly, and satisfy

$$\begin{cases} 1 > 0 \\ \beta_{01}\frac{\kappa+1}{2}|e_1|^{\frac{\kappa-1}{2}} > 0 \\ \beta_{02}\frac{\kappa+1}{2}|e_1|^{\frac{\kappa-1}{2}} > 0, \\ \beta_{03}\frac{\kappa+1}{2}|e_1|^{\kappa-1} > 0 \\ \beta_{01}\beta_{02}\frac{\kappa+1}{2} - \beta_{03} > 0 \end{cases}$$

then it can be considered that A is Hurwitz. According to Lyapunov theory, there exists solution P in Eq. (37). Thus, it is easy to get

$$V_1 = -\varsigma^{\mathrm{T}} Q \varsigma \le -\lambda_{\min}\{Q\}\,\|\varsigma\|_2^2 \tag{40}$$

From Eq. (36), V_2 can be re-expressed as

$$\begin{aligned} V_2 &= 2H(\beta_{03}|e_1|^{\frac{\kappa+1}{2}}\operatorname{sgn}(e_1) + 2e_3) \\ &= \begin{bmatrix} 2H & 0 & 4H \end{bmatrix} \begin{bmatrix} |e_1|^{\frac{\kappa+1}{2}}\operatorname{sgn}(e_1) \\ e_2 \\ e_3 \end{bmatrix} \\ &= \begin{bmatrix} 2H & 0 & 4H \end{bmatrix} \varsigma \\ &\le 2\sqrt{5}H_M\|\varsigma\|_2 \end{aligned} \tag{41}$$

Combining Eqs. (37), (40) and (41), we can know

$$\begin{aligned} \dot{V} = V_1 + V_2 &\le -\lambda_{\min}\{Q\}\,\|\varsigma\|_2^2 + 2\sqrt{5}H_M\|\varsigma\|_2 \\ &= -\left(\lambda_{\min}\{Q\}\|\varsigma\|_2 - 2\sqrt{5}H_M\right)\|\varsigma\|_2 \end{aligned} \tag{42}$$

Q is positive definite and nonsingular, then

$$\begin{aligned} \lambda_{\min}\{Q\} &= \sigma_{\min}\{Q\} = \sigma_{\min}\{-A^{\mathrm{T}}P + PA\} \\ &= \sigma_{\min}\{(-A)^{\mathrm{T}}P + ((-A)^{\mathrm{T}}P)^{\mathrm{T}} \\ &= 2\sigma_{\min}\{(-A)^{\mathrm{T}}P\} \\ &\ge 2\sigma_{\min}\{(-A)^{\mathrm{T}}\}\sigma_{\min}\{P\} \\ &= 2\min\{\frac{\kappa+1}{2}|e_1|^{\frac{\kappa-1}{2}}, 1\}\sigma_{\min}\{\Xi\}\lambda_{\min}\{P\} \end{aligned} \tag{43}$$

where

$$\begin{aligned} (-A)^{\mathrm{T}} &= \begin{bmatrix} \frac{\kappa+1}{2}|e_1|^{\frac{\kappa-1}{2}} & 0 & 0 \\ 0 & 1 & 0 \\ 0 & 0 & |e_1|^{\frac{\kappa-1}{2}} \end{bmatrix} \begin{bmatrix} \beta_{01} & \beta_{02} & \beta_{03} \\ -1 & 0 & 0 \\ 0 & -1 & 0 \end{bmatrix} \\ &= \Theta\Xi. \end{aligned}$$

When $|e_1| > 1$, $\|\varsigma\|_2 \ge |e_1|^{\frac{\kappa+1}{2}}$, $\lambda_{\min}\{Q\} \ge (\kappa+1)|e_1|^{\frac{\kappa-1}{2}}\sigma_{\min}\{\Xi\}\lambda_{\min}\{P\}$, thus

$$\begin{aligned} &\lambda_{\min}\{Q\}\|\varsigma\|_2 - 2\sqrt{5}H_M \\ &\quad \ge (\kappa+1)|e_1|^{\kappa}\sigma_{\min}\{\Xi\}\lambda_{\min}\{P\} - 2\sqrt{5}H_M \\ &\quad \ge (\kappa+1)\sigma_{\min}\{\Xi\}\lambda_{\min}\{P\} - 2\sqrt{5}H_M \end{aligned} \tag{44}$$

$$\begin{aligned} \dot{V} &\le -\left(\lambda_{\min}\{Q\}\|\varsigma\|_2 - 2\sqrt{5}H_M\right)\|\varsigma\|_2 \\ &\le -\left((\kappa+1)\sigma_{\min}\{\Xi\}\lambda_{\min}\{P\} - 2\sqrt{5}H_M\right)\|\varsigma\|_2 \\ &\le -\left((\kappa+1)\sigma_{\min}\{\Xi\}\lambda_{\min}\{P\} - 2\sqrt{5}H_M\right)\sqrt{\frac{V}{\lambda_{\max}\{P\}}} \\ &= -\frac{\left((\kappa+1)\sigma_{\min}\{\Xi\}\lambda_{\min}\{P\} - 2\sqrt{5}H_M\right)}{\sqrt{\lambda_{\max}\{P\}}}V^{\frac{1}{2}} \le 0 \end{aligned} \tag{45}$$

Let $\beta_{0i}(i = 1, 2, 3)$ be adjusted properly so that Eq. (44) > 0, that is $(\kappa+1)\sigma_{\min}\{\Xi\}\lambda_{\min}\{P\} > 2\sqrt{5}H_M$. According to Lemma 1, the error system as Eq. (32) can converge to region $|e_1| \le 1$ and satisfy $|\varsigma| \le 1$ in finite time. When error system converges to $|e_1| \le 1$, it is easy to verify $\min\{\frac{\kappa+1}{2}|e_1|^{\frac{\kappa-1}{2}}, 1\} \ge \frac{\kappa+1}{2}$, then we have $\lambda_{\min}\{Q\} \ge (\kappa+1)\sigma_{\min}\{\Xi\}\lambda_{\min}\{P\}$, thus

$$\begin{aligned} &\lambda_{\min}\{Q\}\|\varsigma\|_2 - 2\sqrt{5}H_M \\ &\quad \ge (\kappa+1)|e_1|^{\frac{\kappa+1}{2}}\sigma_{\min}\{\Xi\}\lambda_{\min}\{P\} - 2\sqrt{5}H_M \end{aligned} \tag{46}$$

If the observer gains are chosen properly, then the following inequality is established

$$1 \ge \|\varsigma\|_2 \ge |e_1|^{\frac{\kappa+1}{2}} > \frac{2\sqrt{5}H_M}{(\kappa+1)\sigma_{\min}\{\Xi\}\lambda_{\min}\{P\}} \tag{47}$$

such that $\dot{V} < 0$ is true. The convergence time is

$$T_{fi} \leq \frac{2}{K}(V(\varsigma))^{\frac{1}{2}} \leq \frac{2}{K}(V(\varsigma_0))^{\frac{1}{2}} \tag{48}$$

where $K = \frac{\left((\kappa+1)\sigma_{\min}\{\Xi\}\lambda_{\min}\{P\}-2\sqrt{5}H_M\right)}{\sqrt{\lambda_{\max}\{P\}}}$.

3.2 Angle of attack controller design

Equation (2) can be reformulated as

$$\dot{\alpha} = q + f_\alpha \tag{49}$$

$$\begin{aligned} f_\alpha = &- \tan(\beta)(\cos(\alpha)p + \sin(\alpha)r) + \frac{1}{mV\cos(\beta)} \\ &(-L + mg\cos(\gamma)\cos(\mu)) + \frac{1}{mV\cos(\beta)} \\ &(-T_x\sin(\alpha) + T_z\cos(\alpha)) \end{aligned} \tag{50}$$

Differentiate Eq. (49) and then substituting Eqs. (8) and (20) into it, we can obtain

$$\begin{aligned} \ddot{\alpha} &= \dot{f}_\alpha + \frac{(I_{zz} - I_{xx})pr + I_{xz}(r^2 - p^2)}{I_{yy}} \\ &\quad + (\frac{(m_a + m_T)}{I_{yy}} - b_{0\alpha}v_1) + b_{0\alpha}v_1 \\ &= F_\alpha + b_{0\alpha}v_1 \end{aligned} \tag{51}$$

where v_1 indicates the pitch manipulation torque, which is a combination of the deflection of elevator surface and the nozzles. $b_{0\alpha}$ is an adjustable parameter, and the positive and negative polarity can be determined according to $\frac{(m_a+m_T)}{I_{yy}}$. According to Eq. (51), v_1 firstly appears in the second-order differential of α. Define

$$\begin{cases} y = \alpha \\ x_1 = y \\ x_2 = \dot{y} \\ x_3 = F_\alpha \end{cases} \tag{52}$$

where x_3 is the extended state, which includes model uncertainties and coupling from other channels. Then, the state-space form of Eq. (51) can be described as

$$\begin{cases} \dot{x}_1 = x_2 \\ \dot{x}_2 = x_3 + b_{0\alpha}v_1 \\ \dot{x}_3 = H_\alpha \\ y = x_1 \end{cases} \tag{53}$$

where $b_{0\alpha}$ is an adjustable parameter related to the system, H_α represents the total disturbance. In this way, the original dynamics can be approximated by a second-order integrator plus a total disturbance. The total disturbance causes the system to deviate from the expected second-order integrator. The key to solving the problem is to estimate the total disturbance and eliminate it. The unique advantage of Eq. (53) is that it treats x_3 regardless of its original form. Reference [34] proposed a continuous finite-time convergent differentiator. Based this finite-time convergent differentiator, a finite-time extended state observer is presented as follows.

$$\begin{cases} \dot{z}_1 = z_2 - \beta_{01}|z_1 - x_1|^{\frac{\kappa+1}{2}}\mathrm{sgn}(z_1 - x_1) \\ \dot{z}_2 = z_3 - \beta_{02}|z_1 - x_1|^{\frac{\kappa+1}{2}}\mathrm{sgn}(z_1 - x_1) + b_{0\alpha}v_1 \\ \dot{z}_3 = -\beta_{03}|z_1 - x_1|^{\kappa}\mathrm{sgn}(z_1 - x_1) \end{cases} \tag{54}$$

where κ is a constant number and $\kappa \in (0, 1)$, $\beta_{0i}(i = 1, 2, 3)$ represents the observer gains, and $\mathrm{sgn}(\cdot)$ is symbolic function. The estimation error of extended state observer $e_{1\alpha} = z_1 - x_1$, $e_{2\alpha} = z_2 - x_2$, $e_{3\alpha} = z_3 - F_\alpha$ can be expressed as follows.

$$\begin{cases} \dot{e}_{1\alpha} = e_{2\alpha} - \beta_{01}|z_1 - x_1|^{\frac{\kappa+1}{2}}\mathrm{sgn}(z_1 - x_1) \\ \dot{e}_{2\alpha} = e_{3\alpha} - \beta_{02}|z_1 - x_1|^{\frac{\kappa+1}{2}}\mathrm{sgn}(z_1 - x_1) \\ \dot{e}_{3\alpha} = -\beta_{03}|z_1 - x_1|^{\kappa}\mathrm{sgn}(z_1 - x_1) - H_\alpha \end{cases} \tag{55}$$

When we obtain $z_3 \approx x_3$ by FTESO and use the control signal as

$$v_1 = \frac{-z_3 + u_0}{b_{0\alpha}} \tag{56}$$

where u_0 is a virtual control variable. Then, the original plant can be approximately reformulated as

$$\ddot{y} \approx u_0 \tag{57}$$

The objective is to select u_0 to regulate $e_\alpha = \alpha - \alpha_d$ to zero in a finite time. From reference [27], an improved super-twisting sliding model control law is selected as

$$\begin{cases} u_0(t) = -\lambda|\sigma|^{\frac{1}{2}}\mathrm{sgn}(\sigma) - k_1\sigma + u_1 \\ \dot{u}_1 = -W\mathrm{sgn}(\sigma) - k_2\sigma \end{cases} \tag{58}$$

where $\sigma = e_\alpha + \lambda\dot{e}_\alpha$ represents the sliding surface.

Remark 1 [27]. For the super-twisting sliding mode control law in Eq. (58), if the gains λ, W, k_1, k_2 are chosen properly, it can be proved that the continuous super-twisting sliding mode control injection term $\sigma = \dot{\sigma} = 0$ is satisfied in finite time.

In order to generate the filtering reference maneuver commands and its differential signal, a tracking differentiator (TD) [14] is used, and its form can be expressed as

$$\begin{cases} \dot{s}_{\alpha 1} = s_{\alpha 2} \\ \dot{s}_{\alpha 2} = fhan\,(s_{\alpha 1} - \alpha_d, s_{\alpha 2}, \varepsilon, \eta) \end{cases} \tag{59}$$

where $s_{\alpha 1}$ is the tracking signal for α_d, $s_{\alpha 2}$ is the differential signal of $s_{\alpha 1}$, ε is the speed factor which can determine the convergence speed, η is the filtering factor, and $fhan(\cdot)$ represents an optimal synthetic function which is constructed as

$$\begin{cases} d = \varepsilon\eta^2 \\ a_0 = \eta s_{\alpha 2} \\ y = (s_{\alpha 1} - \alpha_d) + a_0 \\ a_1 = \sqrt{d\,(d + 8|y|)} \\ a_2 = a_0 + \mathrm{sgn}(y)(a_1 - d)/2 \\ a = (a_0 + y)\,fsg(y, d) + a_2(1 - fsg(y, d)) \\ fsg(x, d) = (\mathrm{sgn}(x + d) - \mathrm{sgn}(x - d))/2 \\ fhan = -\varepsilon(\frac{a}{d})fsg(a, d) - r\,\mathrm{sgn}(a)(1 - fsg(a, d)) \end{cases} \tag{60}$$

3.3 Sideslip angle controller design

Equation (3) can be reformulated as

$$(\dot{\beta}) = -r\cos(\alpha) + f_\beta \tag{61}$$

$$\begin{aligned} f_\beta =& p\sin(\alpha) + \frac{1}{mV}(Y\cos(\beta) + mg\cos(\gamma)\sin(\mu)) \\ &+ \frac{1}{mV}(-T_x\sin(\beta)\cos(\alpha) + T_y\cos(\beta) \\ &- T_z\sin(\beta)\sin(\alpha)) \end{aligned} \tag{62}$$

Due to the symmetry of angle of attack and sideslip angle, the virtual control law for sideslip angle β can be given directly as

$$v_2 = \frac{u_{0\beta} - z_{3\beta}}{b_{0\beta}} \tag{63}$$

where $z_{3\beta}$ can be obtained by

$$\begin{cases} \dot{z}_{1\beta} = z_{2\beta} - \beta_{01}|z_{1\beta} - x_1|^{\frac{\kappa+1}{2}}\mathrm{sgn}(z_{1\beta} - x_1) \\ \dot{z}_{2\beta} = z_{3\beta} - \beta_{02}|z_{1\beta} - x_1|^{\frac{\kappa+1}{2}}\mathrm{sgn}(z_{1\beta} - x_1) + b_{0\beta}v_2 \\ \dot{z}_{3\beta} = -\beta_{03}|z_{1\beta} - x_1|^{\kappa}\mathrm{sgn}(z_{1\beta} - x_1) \end{cases} \tag{64}$$

Define $e_\beta = \beta - s_{1\beta}$, the finite-time feedback control law is designed as

$$\begin{cases} u_{0\beta}(t) = -\lambda_\beta|\sigma|^{\frac{1}{2}}\mathrm{sgn}(\sigma) - k_{1\beta}\sigma + u_{1\beta} \\ \dot{u}_{1\beta} = -W_\beta\mathrm{sgn}(\sigma) - k_{2\beta}\sigma \end{cases} \tag{65}$$

where $\sigma = e_\beta + \lambda_\beta\dot{e}_\beta$. $s_{1\beta}$ is produced by TD

$$\begin{cases} \dot{s}_{\beta 1} = s_{\beta 2} \\ \dot{s}_{\beta 2} = fhan\left(s_{\beta 1} - \beta_d, s_{\beta 2}, \varepsilon, \eta\right) \end{cases} \tag{66}$$

3.4 Roll angular rate controller design

In practical flight, the bank angle μ cannot be measured accurately. Considering this situation, we regulate the roll angular rate p to track an appropriate curve such that can change as expected. Equation (7) can be rewritten as

$$\dot{p} = F_p + b_{0p}v_3 \tag{67}$$

$$\begin{aligned} F_p =& \frac{I_{xz}(n + n_T)}{I_{xx}I_{zz} - I_{xz}^2} + \frac{I_{xz}(I_{xx} - I_{yy} + I_{zz})}{I_{xx}I_{zz} - I_{xz}^2}pq \\ &+ \frac{I_{zz}(I_{yy} - I_{zz}) - I_{xz}^2}{I_{xx}I_{zz} - I_{xz}^2}qr \\ &+ (\frac{I_{zz}}{I_{xx}I_{zz} - I_{xz}^2} - b_{0p})(l + l_T) \end{aligned} \tag{68}$$

Define $x_1 = p, x_2 = F_p, \dot{F}_p = H_p$, the extended state-space expression for the roll angular dynamics can be established as

$$\begin{cases} \dot{x}_1 = x_2 + b_{0p}v_3 \\ \dot{x}_2 = H_p \\ y = x_1 \end{cases} \tag{69}$$

Thus, the corresponding FTESO can be designed as

$$\begin{cases} \dot{z}_{1p} = z_{2p} - \beta_{01p}|z_{1p} - x_1|^{\frac{\kappa+1}{2}}\mathrm{sgn}(z_{1p} - x_1) + b_{0p}v_3 \\ \dot{z}_{2p} = -\beta_{02p}|z_{1p} - x_1|^{\kappa}\mathrm{sgn}(z_{1p} - x_1) \end{cases} \tag{70}$$

Define the estimation error of extended state observer $e_1 = z_{1p} - x_1, e_2 = z_{2p} - F_p$, then the estimation error system can be expressed as follows.

$$\begin{cases} \dot{e}_{1p} = e_{2p} - \beta_{01p}|z_{1p} - x_1|^{\frac{\kappa+1}{2}}\mathrm{sgn}(z_{1p} - x_1) \\ \dot{e}_{2p} = -\beta_{02p}|z_{1p} - x_1|^{\kappa}\mathrm{sgn}(z_{1p} - x_1) - H_p \end{cases} \tag{71}$$

When total disturbance z_{2p} is estimated by FTESO and then compensated by

$$v_3 = \frac{u_{0p} - z_{2p}}{b_{0p}} \tag{72}$$

For the control law u_{0p} in the roll angular rate channel, we let $e_p = p - s_{p1}$ and then choose $\sigma = e_p$ as the sliding mode surface, where s_{1p} is generated by TD

$$\begin{cases} \dot{s}_{p1} = s_{p2} \\ \dot{s}_{p2} = fhan\left(s_{p1} - p_d, s_{p2}, \varepsilon, \eta\right) \end{cases} \tag{73}$$

The corresponding super-twisting controller can be designed as

$$\begin{cases} u_{0p}(t) = -\lambda_p|\sigma|^{\frac{1}{2}}\mathrm{sgn}(\sigma) - k_{1p}\sigma + u_{1p} \\ \dot{u}_{1p} = -W_p\mathrm{sgn}(\sigma) - k_{2p}\sigma \end{cases} \tag{74}$$

3.5 Control allocation

The output of the control law characterizes the need for the desired torques along the three-axis. The control allocation is to obtain the deflection command of each control surface according to the relationship between the control surface and the desired three-axis torque. Let $x_1 = [p \quad q \quad r]^{\mathrm{T}}, \bar{x} = [V \quad \alpha \quad \beta \quad p \quad q \quad r]^{\mathrm{T}}$, $u = \left[\delta_e \quad \delta_a \quad \delta_r \quad \delta_x \quad \delta_y \quad \delta_z\right]^{\mathrm{T}}$, $F(\bar{x}) = [f_p(\bar{x}) \quad f_q(\bar{x}) \quad f_r(\bar{x})]^{\mathrm{T}}$, according to the deflection of aerodynamic control surfaces and thrust vector nozzles, Eqs. (7), (8) and (9) can be reformulated as

$$\begin{cases} \dot{x}_1 = F(\bar{x}) + G(\bar{x})u \\ y_1 = x_1 \end{cases} \tag{75}$$

where $F(\bar{x})$ and $G(\bar{x})$ are expressed as

$$F(\bar{x}) = \begin{bmatrix} \frac{I_{xz}(I_{xx}-I_{yy}+I_{zz})}{I_{xx}I_{zz}-I_{xz}^2}pq + \frac{I_{zz}(I_{yy}-I_{zz})-I_{xz}^2}{I_{xx}I_{zz}-I_{xz}^2}qr \\ \frac{(I_{zz}-I_{xx})pr+I_{xz}(r^2-p^2)}{I_{yy}} \\ \frac{I_{xx}(I_{xx}-I_{yy})+I_{xz}^2}{I_{xx}I_{zz}-I_{xz}^2}pq - \frac{I_{xz}(I_{xx}-I_{yy}+I_{zz})}{I_{xx}I_{zz}-I_{xz}^2}qr \end{bmatrix} \tag{76}$$

$$G(\bar{x}) = \begin{bmatrix} g_{p\delta_e}(\bar{x}) & g_{p\delta_a}(\bar{x}) & g_{p\delta_r}(\bar{x}) & g_{p\delta_x}(\bar{x}) & g_{p\delta_y}(\bar{x}) & g_{p\delta_z}(\bar{x}) \\ g_{q\delta_e}(\bar{x}) & g_{q\delta_a}(\bar{x}) & g_{q\delta_r}(\bar{x}) & g_{q\delta_x}(\bar{x}) & g_{q\delta_y}(\bar{x}) & g_{q\delta_z}(\bar{x}) \\ g_{r\delta_e}(\bar{x}) & g_{r\delta_a}(\bar{x}) & g_{r\delta_r}(\bar{x}) & g_{r\delta_x}(\bar{x}) & g_{r\delta_y}(\bar{x}) & g_{r\delta_z}(\bar{x}) \end{bmatrix} \tag{77}$$

where $g(\bar{x})$ represents control derivatives with respect to all control surfaces including aerodynamic control surfaces and thrust vectoring nozzles. According to the control design process, $F(\bar{x})$ is included in the total disturbance and ESO can estimate it in real time. Let $v = \left[v_1 \; v_2 \; v_3\right]^{\mathrm{T}}$, the control allocation problem can be described as follows. Assume that the expected virtual control command is $v(t) \in \mathrm{R}^3$, and the deflection of control surface is $u(t) \in \mathrm{R}^6$. Then, for the given virtual control input $v = \left[v_1 \; v_2 \; v_3\right]^{\mathrm{T}}$, the control allocation problem is to solve indefinite equation under mapping relations $G(\bar{x}) : \mathrm{R}^6 \to \mathrm{R}^3$

$$\begin{cases} \dot{x}_1 = F(\bar{x}) + G(\bar{x})u \\ y_1 = x_1 \end{cases} \tag{78}$$

and make $u(t)$ satisfy the constraint

$$\Omega = \left\{u(t) \in \mathrm{R}^6 \,|u_{\min} \le u \le u_{\max}, \Gamma_{\min} \le \dot{u} \le \Gamma_{\max}\right\},$$

where $u_{\min(\max)}$ and $\Gamma_{\min(\max)}$ represent the control surface deflection limitation and its rate of change limitation. Considering that the deflection reduction of the vector nozzle can extend its lifespan, the allocation principle is that the priority of aerodynamic control surface should be higher than the thrust vector nozzles. Then, the control input can be divided into two groups as

$$\begin{cases} u = \left[u_{\text{aero}} \; u_{\text{tv}}\right]^{\mathrm{T}} \\ G(\bar{x}) = \left[G_{\text{aero}} \; G_{\text{tv}}\right] \end{cases} \tag{79}$$

where $u_{\text{aero}} = [\delta_e \quad \delta_a \quad \delta_r]^{\mathrm{T}}, u_{\text{tv}} = \left[\delta_x \quad \delta_y \quad \delta_z\right]^{\mathrm{T}}, G_{\text{aero}}$ and G_{tv} represent the first three columns and the last three columns of the matrix $G(\bar{x})$, respectively. The generalized inverse matrix of G_{aero} and G_{tv} can be obtained as $\mathrm{P}_{\text{aero}} = G_{\text{aero}}^{-1}$, $\mathrm{P}_{\text{tv}} = G_{\text{tv}}^{-1}$, respectively. The actuators are approximated by first-order lags; the position and rate limitations are listed in Table 1.

Let ω_a and ω_t represent the bandwidth of aerodynamic surface and thrust vector surface, respectively. The entire allocation process can be shown in Fig. 3. In allocation process, the aerodynamic control surfaces are used first. In practical flight, the control constraints need to be considered. Within its position and rate limitation, the aerodynamic control surface deflections should attempt to satisfy

$$u_{\text{aero}} = P_{ae}v \tag{80}$$

When the calculated deflections of the aerodynamic control surfaces are within the limitation, the allocation

Table 1 The control surfaces constraints

actuator	bandwidth (rad/s)	rate limit (deg/s)	position limit (deg)
Aileron (δ_a)	20.2	±80	±21.5
Elevator (δ_e)	20.2	±60	±25
Rudder (δ_r)	20.2	±120	±30
Roll (δ_x)	30.2	±150	±20
Yaw (δ_y)	30.2	±150	±20
Pitch (δ_z)	30.2	±150	±20

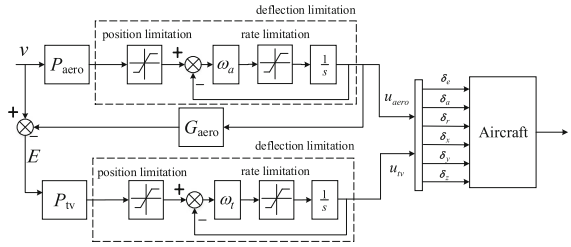

Fig. 3 Control allocation diagram

Table 2 The control parameters

	α	β	p
TD	$\varepsilon = 1, \eta = 0.1$	$\varepsilon = 1, \eta = 0.1$	$\varepsilon = 2, \eta = 0.1$
FTESO	$\beta_{01} = 20,$	$\beta_{01} = 18,$	$\beta_{01} = 16,$
	$\beta_{02} = 120,$	$\beta_{02} = 108,$	$\beta_{02} = 64,$
	$\beta_{03} = 240,$	$\beta_{03} = 216,$	$\kappa = 0.3,$
	$\kappa = 0.6,$	$\kappa = 0.9,$	$b_{0p} = -3.0$
	$b_{0\alpha} = 7.0$	$b_{0\beta} = -1.5$	
SWT	$\lambda = 1.8,$	$\lambda_\beta = 0.8,$	$\lambda_p = 1,$
	$W = 0.4,$	$W_\beta = 0.3,$	$W_\beta = 0.2,$
	$k_1 = 2.5,$	$k_{1\beta} = 0.5,$	$k_{1p} = 2.5,$
	$k_2 = 0.5$	$k_{2\beta} = 0.1$	$k_{2p} = 0.5$

process is over. If u_{aero} reaches the aerodynamic surface saturation, then the thrust vector surface u_{tv} will be added to supplement the allocation error E.

$$\begin{cases} u_{\text{aero}} = Sat_{\text{aero}}(P_{\text{aero}} v) \\ E = v - G_{\text{aero}} u_{\text{aero}} \\ u_{\text{tv}} = Sat_{\text{tv}}(P_{\text{tv}} E) \end{cases} \tag{81}$$

where Sat$((x, \bar{u})$ represents the saturation function as

$$y = \text{Sat}(x, \bar{u}) = \begin{cases} \bar{u} & x > \bar{u} \\ x & -\bar{u} \le x \le \bar{u} \\ -\bar{u} & x < -\bar{u} \end{cases} \tag{82}$$

where $\bar{u}$ represents the upper limitation. In summary, this allocation method maximizes the use of the aerodynamic control surface and reduces the use of the thrust vector control surface.

4 Simulation results

In order to evaluate the effectiveness of the proposed control strategy, the numerical simulations are conducted. The Herbst-type maneuver is selected to verify the control effect of the designed controller. The initial velocity, height and angle of attack are $V = 100\,\text{m/s}$, $h_0 = -z_{E0} = -1200\,\text{m}$ and $\alpha_0 = 10°$, respectively. The controller parameters are tuned as shown in Table 2.

4.1 Performance verification

Case 1: State Tracking and Turning Flight

Herbst maneuver is to complete a small radius turn rapidly at high AOA. In order to verify the performance of the proposed controllers, we choose a Herbst-type maneuver as a benchmark. The termination condition of the Herbst-type maneuver is that the velocity heading angle reverses its direction with a small turning radius. The control objective of the whole maneuver process is to maintain stable tracking of the states α, β and p. In this section, the proposed control strategy is compared with the results of the ADRC method of [44]. Moreover, the conventional sliding mode control (SMC) [45] with finite-time extended state observer (FTESO) is also conducted to stress the advantages of the proposed method.

The simulation results are shown in Figs. 4 and 5. On the whole, the maneuver process can be described as that both the angle of attack and the roll angular rate can track the reference signal, and the sideslip angle is always near zero throughout the maneuvering process. At first, for α and p channel, we let an appropriate curve go through a designed fastest tracking differentiator and use its smooth output as final reference signal shown in Fig. 4a, c, respectively. The angle of attack begins to increase at $t = 1.5$ s and reaches 62°after 2 s and then keeps a certain period of time, while the roll angular rate changes as shown in Fig. 4c to cause the aircraft to realize rolling around the velocity vector. When the rolling is completed, the maneuver ends after the aircraft has been swooped for a while. From Fig. 4a–c, the three control strategies can realize the reference signal tracking, but the proposed method in this paper (SWT + FTESO) can obtain better tracking performance than the other two methods.

In this maneuvering process, the velocity decreases at first and then increases as shown in Fig. 4e. With the changes of α and p, μ changes as bell-shaped curve displayed in Fig. 4d . It is evident from Fig. 4f the heading angle changes 180°which indicates a velocity reversal, and the proposed control method can obtain higher precision. The deflections of engine nozzles are presented in Fig. 5a, and all the controls are within saturation limits. The deflections of aerodynamic control surface are presented in Fig. 5b. The elevator is kept at deflection limitation for a long time, which indicates that the aerodynamic surface is insufficient at low speed and high angle of attack. Although using saturated function instead of sign function, the conventional sliding control method produces some slight chattering in thrust vector nozzles yaw deflection. The control inputs by super-twisting method contain almost no chattering.

Case 2: The Total Disturbance Observation

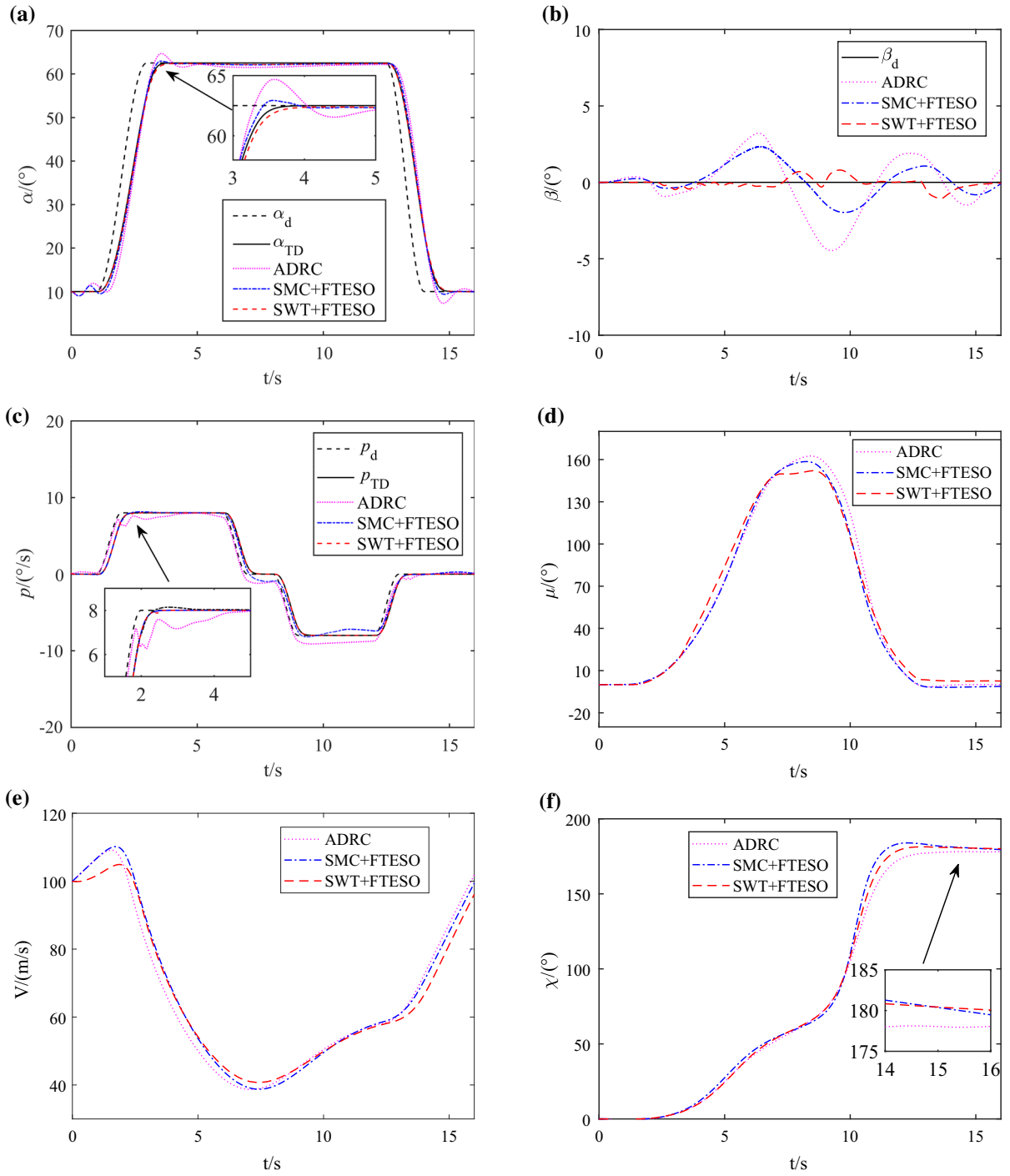

Fig. 4 Herbst-type maneuver. **a** Angle of attack, **b** sideslip angle, **c** roll angular rate, **d** roll angle about the velocity vector, **e** flight speed, **f** velocity heading angle

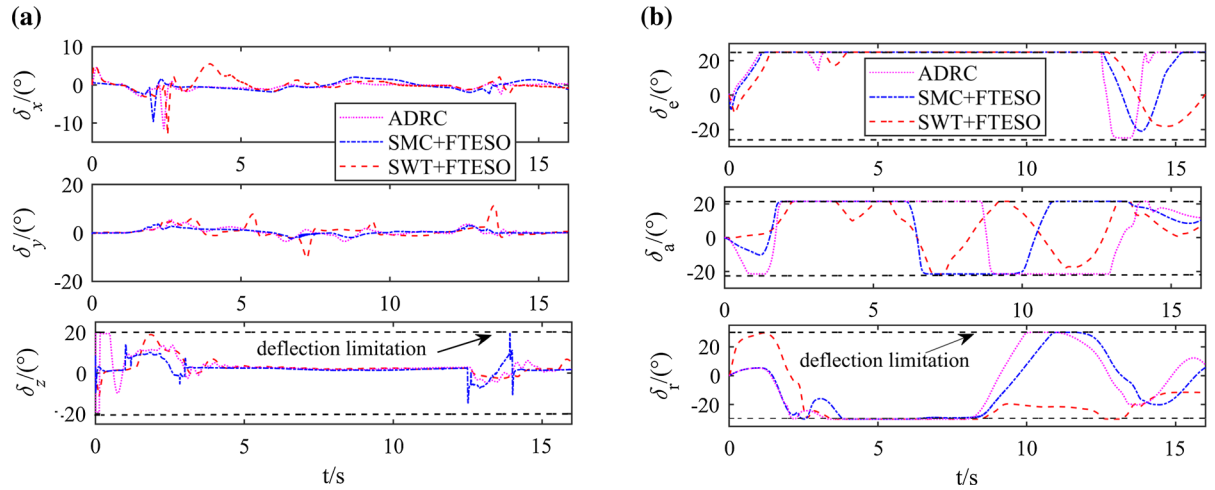

Fig. 5 Control deflections. **a** Thrust vector nozzles deflection, **b** aerodynamic control surfaces deflection

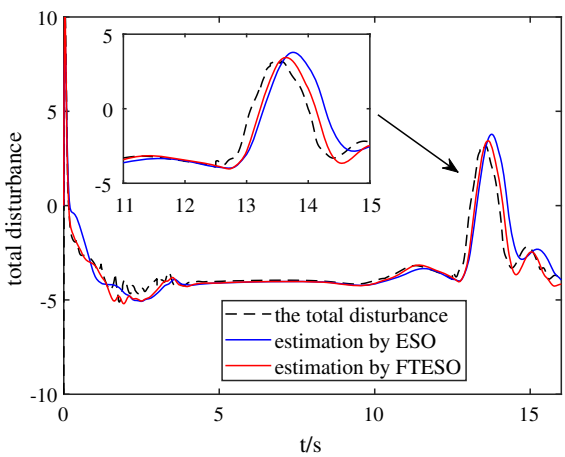

Fig. 6 The total disturbance observation

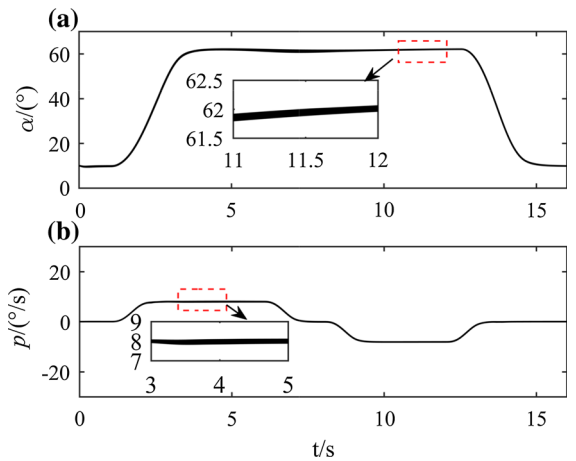

Fig. 7 Monte Carlo simulation. **a** AOA, **b** roll angular rate

To compare the observation ability for the total disturbance between the conventional extended state observer and the finite-time extended state observer, we take the angle of attack channel as an example. When choosing the same output error feedback control law, the estimation of total disturbance is demonstrated in Fig. 6, which indicates that FTESO can obtain better estimation accuracy and smaller estimation delay than the conventional extended state observer.

4.2 Robustness verification

In order to verify the robustness of the proposed controller, a Monte Carlo simulation test is conducted. Forty-three aerodynamic parameters of the nonlinear model are uniformly perturbed within ±30% range, and 500 simulations are conducted together. The results are shown in Figs. 7 and 8, and it is obvious that the response has good consistency and the dynamic performance robustness can be realized.

5 Conclusion

A finite-time control strategy was presented to realize the aircraft high angle of attack maneuver using thrust vector technique. Instead of traditional multivariate control methods, practical decoupling controllers

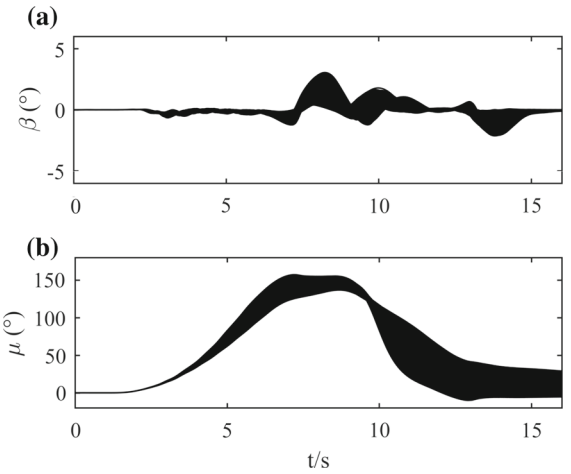

Fig. 8 Monte Carlo simulation. **(a)** sideslip angle, **(b)** bank angle

were designed based on finite-time observers and super-twisting sliding mode controllers. Strong coupling among channels, aerodynamic uncertainties and other unmodeled dynamics were regarded as total disturbance and estimated by a finite-time extended state observer. Daisy chain method was used to achieve control allocation between aerodynamic control surface and thrust vector nozzles. Simulation results demonstrated the effectiveness and robustness of the proposed strategy. In the future, the nonlinear allocation method of aerodynamic control surface and thrust vector can be researched to obtain higher control efficiency. Moreover, the fault tolerance control strategy may be added to improve the performance of aircraft.

Acknowledgements This work was supported by the National Natural Science Foundation of China under Grant Nos. 61973175, 61573197, 61973172 and the Key Technologies R&D Program of Tianjin Grant No. 19JCZDJC32800. The authors thank the editors and the anonymous reviewers for their helpful comments and suggestions that allowed us to improve the paper.

Compliance with ethical standards

Conflict of interest The authors declare that they have no conflict of interest.

Human and animal rights This article does not contain any studies with human participants or animals performed by any of the authors.

Appendix: Nomenclature

Nomenclature	Interpretation
α, β	Angle of attack, sideslip angle
V	Flight speed
g	Gravitational acceleration
μ	Bank angle about the velocity vector
γ	Flight path angle
χ	Velocity heading angle
T	Total engine thrust
$\bar{q}$	Dynamic pressure
I_{xx}, I_{yy}, I_{zz}	Roll, pitch, yaw inertia moments
p, q, r	Components of angular velocity
x_E, y_E, z_E	Position coordinates
C_{x_tot}	Aerodynamic force coefficient in x axis
C_{y_tot}	Aerodynamic force coefficient in y axis
C_{z_tot}	Aerodynamic force coefficient in z axis
C_{l_tot}	Aerodynamic torque coefficient in x axis
C_{m_tot}	Aerodynamic torque coefficient in y axis
C_{n_tot}	Aerodynamic torque coefficient in z axis
T_x, T_y, T_z	Thrust components in three axes
l, m, n	Aerodynamic torque
l_T, m_T, n_T	Thrust vector torque
$\delta_e, \delta_a, \delta_r$	Aerodynamic surfaces deflection angles
$\delta_x, \delta_y, \delta_z$	Thrust vector deflection angles

References

1. Wu, D., Chen, M., Gong, H.: Robust control of post-stall pitching maneuver based on finite-time observers. ISA Trans. **70**(4), 53–63 (2017)
2. Ozgur, A., Kemal, O.: High-alpha flight maneuverability enhancement of a twin engine fighter-bomber aircraft for air combat superiority using thrust-vectoring control, In: AIAA Guidance, Navigation, and Control Conference and Exhibit, pp. 1–26 (2006)
3. Ericsson, L.: Challenges in high-alpha vehicle dynamics. Prog. Aerosp. Sci. **31**(4), 291–334 (1995)
4. Yang, J., Zhu, J.: A hybrid NDI control method for the high-alpha super-maneuver flight control. In: Proceedings of American Control Conference, pp. 6747–6753 (2016)
5. Choudhary, S.K.: Optimal feedback control of a twin rotor MIMO system. Int. J. Simul. Model. **37**(1), 46–53 (2017)
6. Zhang, L., Wang, S., Karimi, H.R., Jasra, A.: Robust finite-time control of switched linear systems and application to a class of servomechanism systems. IEEE-ASME Trans. Mechatron. **20**(5), 2476–2485 (2015)
7. Choudhary, S.K.: Optimal feedback control of twin rotor MIMO system with a prescribed degree of stability. Int. J. Intell. Unman. Syst. **20**(5), 2476–2485 (2015)
8. Snell, S., Enns, D., Garrard, J.: Nonlinear inversion flight control for a supermaneuverable aircraft. J. Guid. Control Dyn. **15**(4), 976–984 (1992)
9. Adams, R., Buffington, J., Banda, S.: Design of nonlinear control laws for high-angle-of-attack flight. J. Guid. Control Dyn. **17**(4), 737–746 (1994)

10. Ronald, H., Cheng, P.: Design for robust aircraft flight control. J. Aircr. **17**(1), 1–12 (2017)
11. Sharma, M.: Flight-path angle control via neuro-adaptive backstepping. In: AIAA Guidance, Navigation, and Control Conference and Exhibit, pp. 1–8 (2002)
12. Sonneveldt, L., Chu, Q., Mulder, J.: Nonlinear flight control design using constrained adaptive backstepping. J. Guid. Control Dyn. **30**(2), 322–336 (2007)
13. Farrell, J., Polycarpou, M., Sharma, M.: Adaptive backstepping with magnitude, rate, and bandwidth constraints: Aircraft longitude control. In: Proceedings of American Control Conference, pp. 3898–3904 (2003)
14. Han, J.: From PID to active disturbance rejection control. IEEE Trans. Ind. Electron. **56**(3), 900–906 (2009)
15. Gao, Z.: On the centrality of disturbance rejection in automatic control. ISA Trans. **53**, 850–857 (2014)
16. Luo, S., Sun, Q., Sun, M., Tan, P., Wu, W., Sun, H., Chen, Z.: On decoupling trajectory tracking control of unmanned powered parafoil using ADRC-based coupling analysis and dynamic feedforward compensation. Nonlinear Dyn. **92**(4), 1619–1635 (2018)
17. Aboudonia, A., El-Badawy, A., Rashad, R.: Active anti-disturbance control of a quadrotor unmanned aerial vehicle using the command-filtering backstepping approach. Nonlinear Dyn. **90**(1), 581–597 (2017)
18. Zhang, C., Yang, J., Li, S., Yang, N.: A generalized active disturbance rejection control method for nonlinear uncertain systems subject to additive disturbance. Nonlinear Dyn. **83**(4), 2361–2372 (2016)
19. Yu, Y., Yuan, Y., Yang, H.: Nonlinear sampled-data ESO-based active disturbance rejection control for networked control systems with actuator saturation. Nonlinear Dyn. **95**(2), 1415–1434 (2019)
20. Raj, K., Muthukumar, V., Singh, S.N., Lee, K.W.: Finite-time sliding mode and super-twisting control of fighter aircraft. Aerosp. Sci. Technol. **82**(5), 487–498 (2018)
21. Utkin, V.I., Guldner, J., Shi, J.: Sliding Modes Control in Electromechanical Systems. Taylor and Francis, London (1999)
22. Emelyanov, S.V., Korovin, S.V., Levantovsky, L.V.: Higher order sliding modes incontrol system. Differ. Equ. **29**(11), 1627–1647 (1993)
23. Defoort, M., Floquet, T., Kokosy, A.: A novel high order sliding mode control scheme. Syst. Control Lett. **58**(2), 102–108 (2009)
24. Levant, A.: Sliding order and sliding accuracy in sliding mode control. Int. J. Control **58**(6), 1247–1263 (1993)
25. Levant, A.: Principles of 2-sliding mode design. Automatica **43**(4), 576–586 (2007)
26. Moreno, J.A., Osorio, M.: Strict Lyapunov functions for the super-twisting algorithm. IEEE Trans. Autom. Control **57**(4), 1035–1040 (2012)
27. Nagesh, I., Edwards, C.: A multivariable super-twisting sliding mode approach. Automatica **50**(3), 984–988 (2014)
28. Defoort, M., Nollet, F., Floquet, T., et al.: A third-order sliding-mode controller for a stepper motor. IEEE Trans. Ind. Electron. **56**(9), 3337–3346 (2009)
29. Mobayen, S., Tchier, F., Ragoub, L.: Design of an adaptive tracker for n-link rigid robotic manipulators based on super-twisting global nonlinear sliding mode control. Int. J. Syst. Sci. **48**(9), 1990–2002 (2017)
30. Haghighi, D.A., Mobayen, S.: Design of an adaptive super-twisting decoupled terminal sliding mode control scheme for a class of fourth-order systems. ISA Trans. **75**, 216–225 (2018)
31. Nasiri, M., Mobayen, S., Zhu, Q.M.: Super-twisting sliding mode control for gearless PMSG-based wind turbine. Complexity, Early Access 1–15 (2019). https://doi.org/10.1155/2019/6141607
32. Qin, Y., Rath, J., Hu, C., Sentouh, C., Wang, R.: Adaptive nonlinear active suspension control based on a robust road classifier with a modified super-twisting algorithm. Nonlinear Dyn. **97**(4), 2425–2442 (2019)
33. Levant, A.: High-order sliding modes, differentiation and output-feedback control. Int. J. Control **76**(9), 924–941 (2003)
34. Wang, X., Lin, H.: Design and frequency analysis of continuous finite-time-convergent differentiator. Aerosp. Sci. Technol. **18**(1), 69–78 (2012)
35. Davila, J., Fridman, L., Levant, A.: Second-order sliding-mode observer for mechanical systems. IEEE Trans. Autom. Control **50**(11), 1785–1789 (2005)
36. Lu, K., Xia, Y.: Finite-time attitude control for rigid spacecraft-based on adaptive super-twisting algorithm. IET Control Theory Appl. **8**(15), 1465–1477 (2014)
37. Levant, A., Pridor, A., Gitizadeh, R., Yaesh, I., Benasher, J.: Aircraft pitch control via second-order sliding technique. J. Guid. Control Dyn. **23**(4), 586–594 (2000)
38. Raj, K., Muthukumar, V., Singh, S.: Robust higher-order sliding mode control systems for roll-coupled maneuvers of aircraft using output feedback. In: Proceedings of 2018 Atmospheric Flight Mechanics Conference, pp. 1–22 (2018)
39. Zong, Q., Dong, Q., Wang, F., Tian, B.: Super twisting sliding mode control for a flexible air-breathing hypersonic vehicle based on disturbance observer. Sci. China Inf. Sci. **58**(7), 1–15 (2015)
40. Jiang, T., Lin, D., Song, T.: Finite-time control for small-scale unmanned helicopter with disturbances. Nonlinear Dyn. **96**(3), 1747–1763 (2019)
41. Stevens, B., Lewis, F.: Aircraft Control and Simulation. Wiley, Hoboken (2007)
42. Basin, M., Yu, P., Shtessel, Y.: Finite- and fixed-time differentiators utilising HOSM techniques. IET Control Theory Appl. **11**(8), 1144–1152 (2016)
43. Bhat, S., Bernstein, D.: Finite-time stability of continuous autonomous systems. SIAM J. Control Optim. **38**(3), 751–766 (2000)
44. Liu, J., Sun, M., Chen, Z., Sun, Q.: Practical coupling rejection control for Herbst maneuver with thrust vector. AIAA J. Aircr. **56**(4), 1726–1734 (2019)
45. Mukherjee, K., Thomas, P., Manoranjan, S.: Automatic recovery of a combat aircraft from a completed cobra and Herbst maneuver: a sliding mode control based scheme. In: Proceedings of 2nd Indian Control Conference, pp. 259–266 (2016)